

10-12

# ORBITAL DEBRIS IMPACT DAMAGE TO REUSABLE LAUNCH VEHICLES

JENNIFER H. ROBINSON

NASA Marshall Space Flight Center, Huntsville, AL 35812 USA

**Summary**—In an effort by the National Aeronautics and Space Administration (NASA), hypervelocity impact tests were performed on thermal protection systems (TPS) applied on the external surfaces of reusable launch vehicles (RLV) to determine the potential damage from orbital debris impacts. Three TPS types were tested, bonded to composite structures representing RLV fuel tank walls. The three heat shield materials tested were Alumina-Enhanced Thermal Barrier-12 (AETB-12), Flexible Reusable Surface Insulation (FRSI), and Advanced Flexible Reusable Surface Insulation (AFRSI). Using this test data, predictor equations were developed for the entry hole diameters in the three TPS materials, with correlation coefficients ranging from 0.69 to 0.86. Possible methods are proposed for approximating damage occurring at expected orbital impact velocities higher than tested, with references to other published work.

## INTRODUCTION

The National Aeronautics and Space Administration (NASA) and private industry are cooperating to develop new design technologies for reusable launch vehicles (RLV). These tasks include the new application of thermal materials for cryogenic insulation and reentry heating insulation on the external surfaces of the RLV's. The RLV's are planned to be in operation for up to twenty years, launching payloads to low earth orbit, including resupply missions to the International Space Station. Program planners predict each vehicle may be in orbit a total of up to five years over its twenty year life. As a consequence of this low earth orbit exposure, the vehicles will be subjected to potentially damaging impacts by manmade orbital debris.

At the NASA/George C. Marshall Space Flight Center (MSFC), the extent of damage orbital debris can cause to RLV thermal protection systems (TPS) is being studied. In 1994 and 1995, two series of hypervelocity impact tests on preliminary RLV TPS/structure designs were completed. The original purpose of the tests was to determine the ballistic limit for each TPS/composite tank wall design. The test results, damage morphologies, ballistic limits and related penetration probabilities are given in References [1-3]. These same data sets are used in this paper to determine predictor equations for hypervelocity particle entry hole diameters in the TPS tiles and blankets. The TPS includes the cryogenic insulation and the outer heat shield material, bonded to a composite load-carrying structure. In most of the configurations tested, this structure was integral with the pressurized fuel tanks, as shown in Figure 1. Perforation of the heat shield materials by orbital particles could lead to catastrophic failure of the vehicle from penetration of the fuel tank, or during reentry heating of the load-carrying structure.

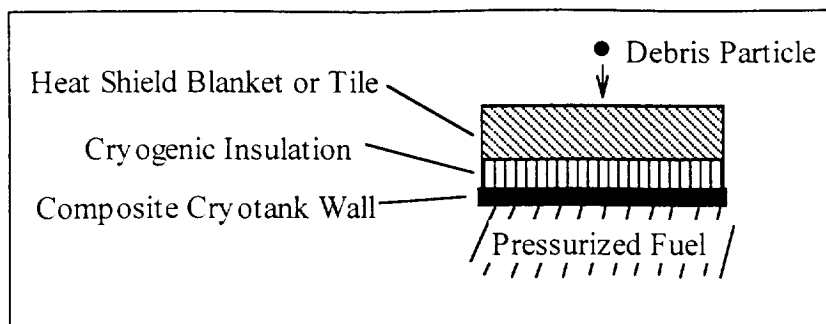


Fig. 1. Typical RLV integral tank cross-section.

## TPS AND TANK WALL MATERIALS

Three heat shield materials were included in this study: AETB, Alumina-Enhanced Thermal Barrier-12 ( $0.192 \text{ g/cm}^3$ ); FRSI, Flexible Reusable Surface Insulation, a Nomex felt ( $0.134 \text{ g/cm}^3$ ); and AFRSI, Advanced Flexible Reusable Surface Insulation ( $0.160 \text{ g/cm}^3$ ; avg. break strength assumed  $813.73 \text{ kg/cm}^2$ ). Material thicknesses varied from 0.64 to 7.62 cm. The TUFİ coating, Toughened Uni-Piece Fibrous Insulation, coated on the surfaces of the AETB tiles was approximately 0.25 cm thick and approximately  $1.32 \text{ g/cm}^3$  (strength approximately  $52.73 \text{ kg/cm}^2$ ).

The cryofoam used in the test sample construction was Rohacell, a rigid, structural, closed cell polymethacrylimide (PMI) foam. Rohacell 51WF ( $0.051 \text{ g/cm}^3$ ) was in all but two test samples which contained Rohacell 71WF ( $0.075 \text{ g/cm}^3$ ).

Two types of composite cryogenic tank walls were tested: 0.23 cm 16-ply IM7/8552 graphite/epoxy ( $1.6 \text{ g/cm}^3$ ); and 0.15 or 0.11 cm thick IM7/8552 graphite/epoxy ( $1.6 \text{ g/cm}^3$ ) face sheets sandwiched around the cryofoam.

3M Nextel® 440 ceramic fabric (0.10 cm thick, 12 harness satin weave, non-standard product,  $0.719 \text{ g/cm}^3$ ) and high strength Hexcel Kevlar® 49 fabric (0.03 cm thick, 285 crowfoot weave,  $1.24 \text{ g/cm}^3$ ) were interlayered between heat shield and cryofoam layers in several of the samples to attempt to increase the penetration resistance of the samples. Earlier orbital debris shield design studies indicated that Nextel® and Kevlar® increased penetration resistance when used in certain structural configurations [4-8].

The components of each test sample were bonded together with thin layers of RTV (room temperature vulcanizing) adhesive.

The outer walls of some of the non-integral tank configurations consisted of a heat resistant blanket or tile bonded to composite facesheet honeycomb panels with 0.040 cm IM7/5250-4 graphite/BMI face sheets ( $1.66 \text{ g/cm}^3$ ) and a 1.27 cm Nomex honeycomb core (assumed  $0.048 \text{ g/cm}^3$ ). For the remaining non-integral tank configurations, the heat resistant blankets or tiles were bonded to an outer single-thickness wall of 0.10 cm thick IM7/5250-4 graphite/BMI panel ( $1.66 \text{ g/cm}^3$ ).

All the materials except the composite panels were typically 15.2 cm square. The composite cryotank wall panels and the non-integral composite structure panels, when used, were 25.4 cm square. Spacing between the composite panels in the non-integral configurations varied between 15.2 and 20.3 cm, as specified in the sketches accompanying the tables describing individual test specimens, in the following sections.

## TEST DESCRIPTION

The HVI tests were performed at NASA/Marshall Space Flight Center at the Space Debris Impact Facility [9]. The facility consists of an instrumented two-stage light gas gun (LGG) capable of launching 0.3175 to 1.27 cm diameter particles from 3 to 7 km/sec. Projectile velocity is measured with a pulsed x-ray system and a Hall photographic station. 1100-O aluminum ( $2.71 \text{ g/cm}^3$ ) spherical projectiles at approximately 6 km/sec were used for each test. For this test series, the intermediate test chamber (.66 m X .66 m X 1.2 m) was utilized. The barrel and test chamber were pumped to a vacuum of 400 milli-Torr for each test.

Aluminum 2024-T3 witness plates ( $2.77 \text{ g/cm}^3$ ) were held in place behind each test sample during impact, as shown in Figure 2. Each witness plate was 0.05 cm thick, and spaced 5.1 cm from the back of the test sample, and 5.1 cm between additional witness plates.

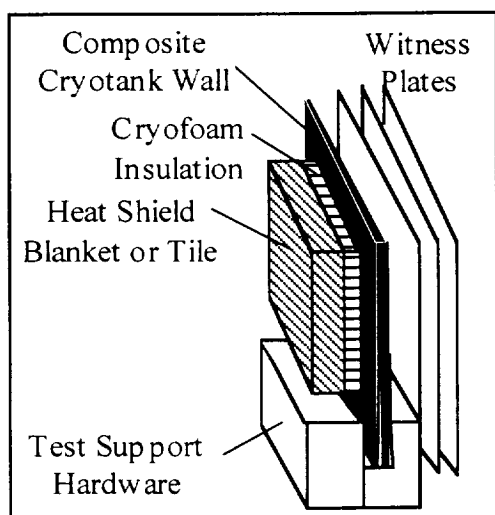


Fig. 2. Typical test setup.

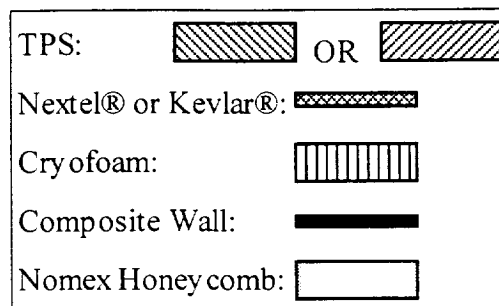


Fig. 3. Materials for table sketches.

## TEST DATA REGRESSION RESULTS

Equations were developed for each of the three heat shield materials: AETB, FRSI, and AFRSI, to predict the entry hole diameters formed at the test particle impact velocity. These diameters were measured in-plane with the outer surface of the blanket or tile. The parameters chosen for the equations were those shown to be significant in previous hypervelocity impact studies, as they seemed appropriate in each material's impact process. Non-dimensional analysis methods were the basis for the regressions performed. Most tests were normal surface impacts; #1610 (an AFRSI configuration) was  $30^\circ$  off normal.

Tables describe the test samples, test parameters and results. Where "N" or "K" are shown within the tables indicates the use and location of single Nextel® or Kevlar® blankets. For example, from Table 1, test sample #1652 consisted of 0.41 cm of FRSI, a layer of Nextel® fabric, another layer of 0.81 cm thick FRSI, a layer of Kevlar® fabric, 1.27 cm of cryofoam, and finally the composite cryotank wall. The sketches corresponding to each configuration tested use the material designations shown in Figure 3. The sketches are not to scale, but are simply intended to show the stacking order of the materials in each test sample.

## FRSI Regression Results

Table 1 includes sketches of each of the seven FRSI configurations tested, the test sample material thicknesses, and the test parameters and resulting damage to FRSI.

Equation (1) is the predictor equation for the entry hole diameter in the FRSI heat blanket material, formed by entry of the hypervelocity particle at approximately 6 km/s. The sketches in Figure 4 illustrate the configurations for FRSI used to develop Equation (1). The correlation coefficient for this equation is 0.69 for 17 data points.

$$H = 1.261 \{ t_1^{3.068} (t_2/t_1)^{0.5513} (d/t_1)^{1.880} (r_1/r_p)^{-1.352} (r_2/r_p)^{0.9380} \}^{0.326} \quad (1)$$

where:  $H$  = clear entry hole diameter in FRSI, cm  
 $t_1$  = thickness of first FRSI blanket, cm  
 $t_2$  = thickness of second layer (FRSI blanket or Nextel®), if any, cm  
 $d$  = particle diameter, cm  
 $r_p$  = particle material density, g/cm<sup>3</sup>  
 $r_1$  = material density of FRSI, g/cm<sup>3</sup>  
 $r_2$  = material density of  $t_2$ , if any, g/cm<sup>3</sup>  
 (for impact velocities 5.5 km/sec  $\leq v \leq$  6.5 km/sec, only)

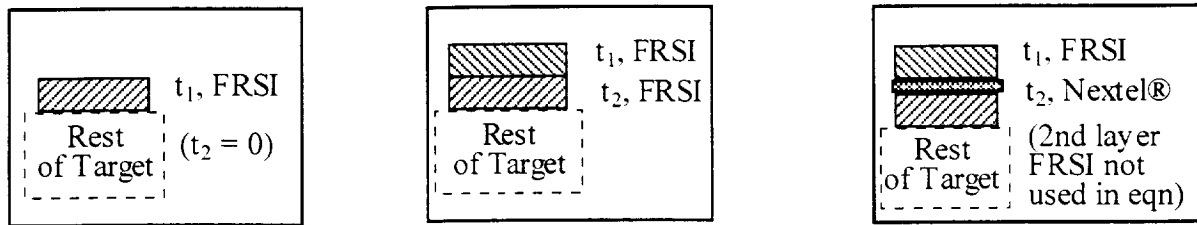


Fig. 4. FRSI configurations.

The parameters chosen for regression of the FRSI data were: particle diameter and material density; and target material thicknesses and densities. Since including impact velocity in the regression produced a very low correlation coefficient, it was dropped as a parameter. The angle of particle impact was not included, since all tests were normal impacts. Due to the felt-like structure of the FRSI, the actual diameter of deformed or damaged material extended out from the clear hole, shown in Figure 5. The material density of FRSI is assumed to be constant throughout the blanket thickness.

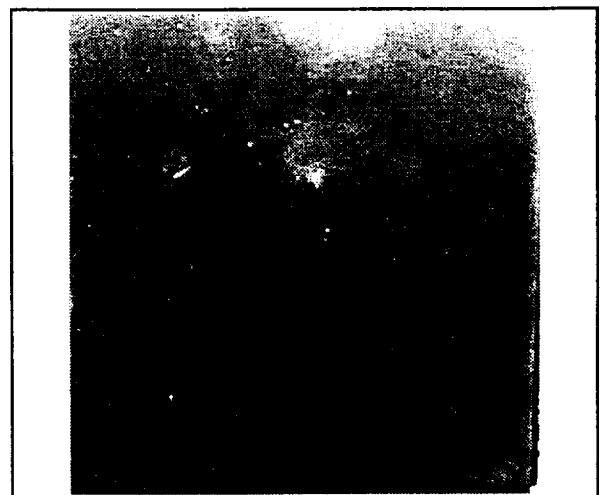
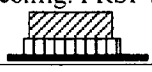

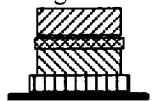
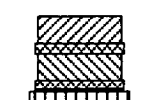
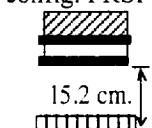
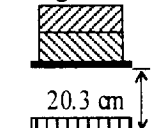



Fig. 5. Damage to #1615 FRSI blanket.

Table 1. FRSI test samples, test parameters and results

	Test #	Material Thickness, cm				Test Parameters & Results		
		FRSI	Cryofoam	Composite Outer Shell	Composite Tank Wall	Particle Diam.,cm	Velocity, km/sec	Hole Diam.,cm
	1612	0.89	2.03	-	0.23	0.32	6.07	0.86
	1613	1.27	1.27	-	0.23	0.32	6.30	1.02
	1615	1.27/N	1.27	-	0.23	0.32	6.30	1.02
	1634	.41/N/.81	1.91	-	0.23	0.47	6.22	1.83
	1641	.41/N/.81	1.91	-	0.23	0.32	6.18	1.52
	1668	.41/N/.81	1.91 (71WF)	-	0.23	0.47	5.96	1.04
	1670	.41/N/.81	1.91 (71WF)	-	0.23	0.32	6.03	1.02
	1650	.41/N/.81/K	1.27	-	0.23	0.47	approx. 6	1.30
	1652	.41/N/.81/K	1.27	-	0.23	0.64	6.16	1.50
	1653	.81/N/.81/K	1.27	-	0.23	0.47	6.23	1.32
	1656	.81/N/.81/K	1.27	-	0.23	0.47	approx. 6	1.40
	1624	0.91	1.78	.04/.04	0.23	0.64	6.00	2.54
	1630	0.70	1.78	.04/.04	0.23	0.47	6.35	2.29
	1659	.41/.81	1.91	.10	0.23	0.32	6.11	0.99
	1660	.41/.81	1.91	.10	0.23	0.47	6.00	1.17
	1675	.41/.81	1.27	-	.11/.11	0.47	5.95	2.29
	1676	.41/.81	1.27	-	.11/.11	0.32	6.23	0.69

### AFRSI Regression Results

Table 2 includes sketches of each of the eight AFRSI configurations tested, the test sample material thicknesses, and the test parameters and resulting damage to AFRSI.

Equation (2) is the predictor equation for the entry hole diameter in the AFRSI heat blanket material, formed by entry of the hypervelocity particle at 6 km/s. The sketches in Figure 6 illustrate the configurations for AFRSI used to develop Equation (2). The correlation coefficient for this equation is 0.69 for 28 data points.

$$H = 1.615 \{ t_1^{1.381} (t_2/t_1)^{-0.340} (d/t_1)^{1.328} (k/v)^{0.496} (r_1/r_p)^{-0.339} (r_2/r_p)^{-0.444} \}^{0.724} \quad (2)$$

where: H = clear entry hole diameter in AFRSI, cm  
 $t_1$  = AFRSI quartz cloth, or Nextel<sup>®</sup> thickness, cm

$t_2$  = Remainder of AFRSI or entire AFRSI thickness, cm

$d$  = particle diameter, cm

$r_p$  = particle material density, g/cm<sup>3</sup>


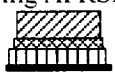



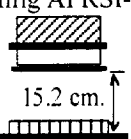
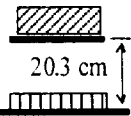

$r_1$  = material density of the AFRSI quartz cloth, or Nextel<sup>®</sup>, g/cm<sup>3</sup>

$r_2$  = material density of the AFRSI, g/cm<sup>3</sup>

$v$  = particle velocity, 5.5 km/s  $\leq v \leq$  6.5 km/s only, km/s

$k$  = material variable (0.288 for AFRSI quartz cloth, or 0.170 for Nextel<sup>®</sup>), km/s

Table 2. AFRSI test samples, test parameters and results

	Test #	Material Thickness, cm				Test Parameters & Results		
		AFRSI	Cryofoam	Composite Outer Shell	Composite Tank Wall	Particle Diam.,cm	Velocity, km/sec	Hole Diam.,cm
config AFRSI-1 	1603	1.27	1.27	-	0.23	0.32	6.20	1.04
	1605	2.54	1.91	-	0.23	0.32	6.80	1.02
	1606	2.54	1.91	-	0.23	0.64	5.88	1.52
	1607	2.54	1.91	-	0.23	0.47	5.91	1.73
	1608	1.27	1.27	-	0.23	0.32	6.20	0.66
	1678	1.27	1.27	-	0.23	0.32	6.11	1.02
config AFRSI-2 	1604	1.27/N	1.27	-	0.23	0.32	6.30	0.97
	1609	1.27/N	1.27	-	0.23	0.47	6.06	1.57
	1610	1.27/N	1.27	-	0.23	0.47	5.97, 30°	1.47
config AFRSI-3 	1635	N/1.91	1.91	-	0.23	0.47	6.20	1.30
config AFRSI-4 	1637	N/1.91/N	1.91	-	0.23	0.47	6.20	1.30
config AFRSI-5 	1654	N/2.54/K	1.27	-	0.23	0.47	5.93	1.09
	1655	N/2.54/K	1.27	-	0.23	0.47	5.91	0.76
	1657	N/2.54/K	1.91	-	0.23	0.47	approx. 6	0.89
	1658	N/2.54/K	1.91	-	0.23	0.47	6.16	0.91
	1665	N/5.08/K	1.91	-	0.23	0.64	6.16	1.14
	1667	N/5.08/K	1.91	-	0.23	0.47	5.92	0.81
	1672	N/2.54/K	1.27	-	0.23	0.47	5.85	1.07
	1673	N/2.54/K	1.27	-	0.23	0.47	5.76	1.02
config AFRSI-6 	1631	0.64	1.78	.04/.04	0.23	0.47	6.20	2.36
	1632	1.27	1.27	.04/.04	0.23	0.64	5.83	1.78
config AFRSI-7 	1661	1.91	1.91	.10	0.23	0.47	approx. 6	1.52
	1663	1.91	1.91	.10	0.23	0.64	approx. 6	1.73
config AFRSI-8 	1674	2.54	1.27	-	.15/.15	0.47	5.83	0.97
	1677	2.54	1.27	-	.15/.15	0.32	6.06	0.64
	1642	2.54	1.91	-	.11/.11	0.32	6.45	0.97
	1643	5.08	1.91	-	.11/.11	0.32	6.31	1.14
	1671	2.54	1.27	-	.11/.11	0.47	5.97	1.80

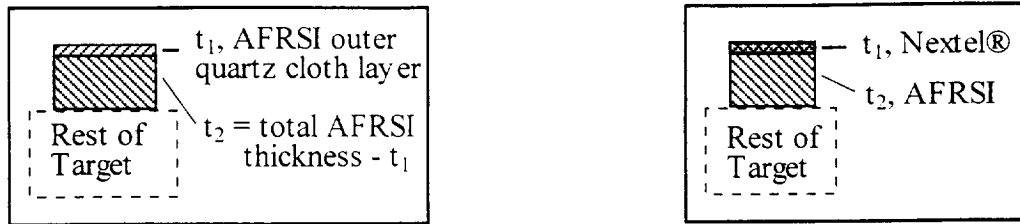


Fig. 6. AFRSI configurations.

The parameters chosen for the regression of the AFRSI data were: particle diameter, material density and velocity; target material thicknesses, densities and the material variable,  $k = [\text{material strength} \times (9.8 \text{ m/s}^2) / \text{material density}]^{0.5}$ . Unlike the FRSI regression, including the impact velocity did not cause a lower correlation with the data; therefore it was retained in the equation. However, this does not imply the equation can be extrapolated outside the range of velocities tested. The angle of particle impact was not included, since all but one test was normal to the surface. Because the outer surface of AFRSI blankets is a woven cloth, the actual diameter of deformed or damaged material cannot be accurately measured; measurements were made to approximate the clear circular hole diameter through the cloth. The blanket consists of a 0.07 cm thick quartz fabric (0.94 g/cm<sup>3</sup>) sewn around an internal thickness of felt (assumed same density as complete AFRSI blanket, 0.160 g/cm<sup>3</sup>). Figure 7 shows typical hypervelocity impact damage on an AFRSI blanket. Additional test results for AFRSI blankets can be found in Reference [10], along with a proposed ballistic limit predictor equation for AFRSI blankets bonded to a substrate.

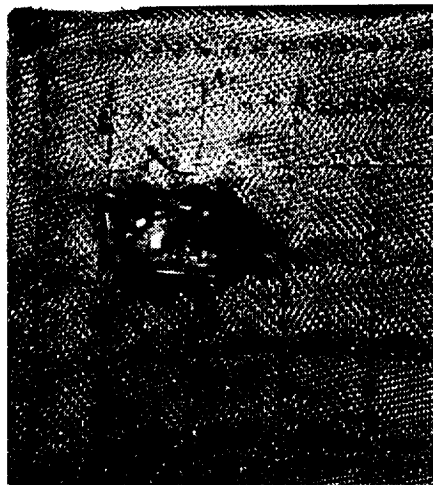


Fig. 7. Damage to #1603 AFRSI blanket.

### AETB Regression Results

Table 3 includes sketches of each of the three AETB configurations tested, the test sample material thicknesses, and the test parameters and resulting damage to AETB.

Equation (3) is the predictor equation for the entry hole diameter in the AETB (0.192 g/cm<sup>3</sup>) heat tile, formed by entry of the hypervelocity particle at approximately 6 km/sec. The sketches in Figure 8 illustrate the configurations for AETB used to develop Equation (3). The

correlation coefficient for this equation is 0.86 for 10 data points. The improved correlation over the FRSI and AFRSI is probably due to less subjectivity in measurement of the damage in the hard AETB tile. Also, the material density used is likely closer to the actual value than those used for the loosely packed flexible blankets.

$$H = 0.845 \{ (t_1)^{3.477} (t_2/t_1)^{-1.756} (d/t_1)^{3.153} (k/v)^{-0.072} (r_1/r_p)^{2.163} (r_2/r_p)^{-2.753} \}^{0.288} \quad (3)$$

where:  $H$  = clear entry hole diameter in AETB, cm  
 $t_1$  = estimated AETB coating (TUF) thickness, cm  
 $t_2$  = total AETB thickness minus coating thickness (0.03 cm), cm  
 $d$  = particle diameter, cm  
 $r_p$  = particle material density, g/cm<sup>3</sup>  
 $r_1$  = material density of the TUF coating, g/cm<sup>3</sup>  
 $r_2$  = material density of the AETB, g/cm<sup>3</sup>  
 $v$  = particle velocity, 5.5 km/sec  $\leq v \leq$  6.5 km/sec only, km/s  
 $k$  = material variable ( 0.06307 for AETB's TUF coating), km/s

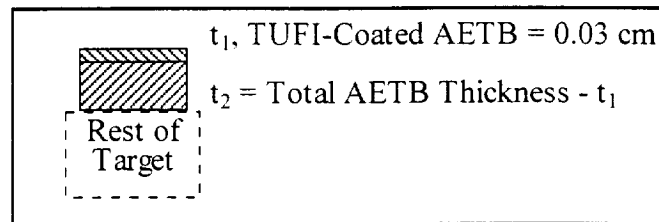


Fig. 8. AETB configuration.

Table 3. AETB test samples, test parameters and results

	Test #	Material Thickness, cm				Test Parameters & Results		
		AETB	Cryofoam	Composite Outer Shell	Composite Tank Wall	Particle Diam., cm	Velocity, km/sec	Hole Diam., cm
config AETB-1 	1616	5.08	1.78	-	0.23	0.32	6.10	1.02
	1617	5.08	1.78	-	0.23	0.64	5.60	1.78
	1618	6.35	2.54	-	0.23	0.64	5.88	1.91
	1619	6.35	2.54	-	0.23	0.95	6.02	3.96
	1620	6.35	2.54	-	0.23	0.80	5.91	2.29
	1621	5.08	1.78	-	0.23	0.80	5.98	2.54
	1625	7.62	3.05	-	0.23	0.80	6.05	2.54
	1626	7.62	3.05	-	0.23	0.95	6.53	NotAvail
config AETB-2 	1622	1.27	1.27	0.04/0.04	0.23	0.95	6.35	NotAvail
	1623	1.27	1.27	0.04/0.04	0.23	0.80	6.10	6.35
config AETB-3 	1662	5.08	1.91	0.11	0.23	0.64	6.10	1.91
	1664	5.08	1.91	0.11	0.23	0.80	5.99	2.18



The parameters chosen for the regression of the AETB data were: particle diameter, material density and velocity; material thicknesses, densities and the material variable,  $k = [\text{material strength} \times (9.8 \text{ m/s}^2) / \text{material density}]^{0.5}$ . As in the AFRSI regression, including the impact velocity did not cause a lower correlation with the data; therefore it was retained in the equation. However, this does not imply the equation can be extrapolated outside the range of velocities tested. The angle of particle impact was not included, since all tests were normal impacts. Figure 9 illustrates typical front surface damage seen in TUFI-coated AETB tiles. Discussion of the damage morphology seen on the test samples was previously published in Reference [1] and is not discussed in detail here. However, several other recent publications show similar reflected-cone-shaped damage in materials with densities of  $0.14 \text{ g/cm}^3$  [11], and  $0.3 \text{ g/cm}^3$  and  $1.9 \text{ g/cm}^3$  [12]. The shape seems due to debris cloud expansion after initial impact, followed by a decrease in energy as it passes through the thickness of the tile. Figure 10 is a simple sketch of this damage shape. Reference [10] also describes a similar damage shape, in addition to a proposed ballistic limit predictor equation for TUFI-coated AETB tiles bonded to a substrate.

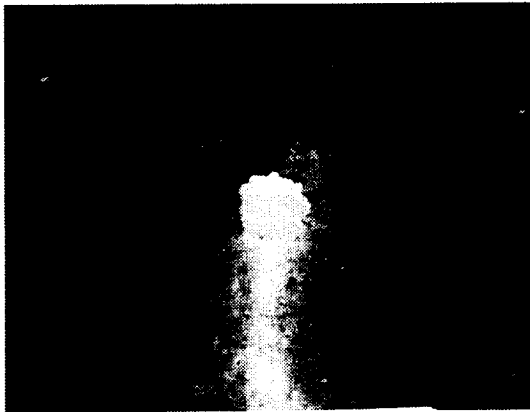


Fig. 9. Damage to #1617 AETB tile.

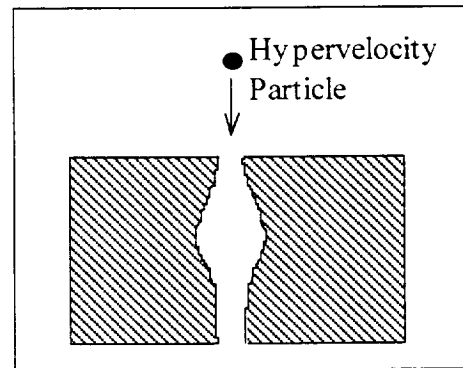


Fig. 10. Typical shape of internal AETB tile damage.

## Composite Cryotank Wall Test Results

Several efforts were made to regress the composite cryotank data to form a predictor equation for the hole diameter in the wall. Although the resulting equations mathematically correlated well to the data, too many inconsistencies existed in the equations to allow for publication. With the presentation of the data here, interested researchers may be able to develop an adequate predictor equation. The data presented in Table 7 includes both the integral and non-integral tank configurations; the non-integral configurations are shaded. Sketches of each configuration, and material thicknesses can be found in previous sections of this paper. Typical damage seen in the graphite/epoxy laminate panels [1] was consistent with that reported by Yew and Kendrick [13].

Table 7. Test parameters and composite tank wall results

TPS Type	Test #	AI Particle Diameter, cm	Velocity, km/sec	Impact Angle, degrees	Composite Tank Wall Damage
FRSI	1612	0.32	6.07	0	1.3 x 0.7 cm Hole
	1613	0.32	6.30	0	1.0 cm Hole
	1615	0.32	6.30	0	Rear-side Delam.
	1634	0.47	6.22	0	1.5 x 2.7 cm Hole
	1641	0.32	6.18	0	None Visible
	1668	0.47	5.96	0	1.7 x 3.2 cm Hole
	1670	0.32	6.03	0	Delam., No Hole
	1650	0.47	approx. 6	0	2.1 x 3.3 cm Hole
	1652	0.64	6.16	0	3.4 x 3.9 cm Hole
	1653	0.47	6.23	0	1.0 x 1.4 cm Hole
	1656	0.47	approx. 6	0	2.0 x 2.3 cm Hole
	1624	0.64	6.00	0	4.3 cm Irreg. Hole
	1630	0.47	6.35	0	None Visible
	1659	0.32	6.11	0	None Visible
	1660	0.47	6.00	0	None Visible
	1675	0.47	5.95	0	3.6 x 2.3 cm Hole
AETB	1676	0.32	6.23	0	2.0 cm Long Crack
	1616	0.32	6.10	0	None Visible
	1617	0.64	5.60	0	None Visible
	1618	0.64	5.88	0	None Visible
	1619	0.95	6.02	0	6.4 x 15 cm Hole
	1620	0.80	5.91	0	0.8 x 1.0 cm Hole
	1621	0.80	5.98	0	3.8 x 7.6 cm Hole
	1625	0.80	6.05	0	None Visible
	1626	0.95	6.53	0	Entire Panel Delaminated
	1622	0.95	6.35	0	6.4 x 3.3 cm Hole
	1623	0.80	6.10	0	6 Small Holes
	1662	0.64	6.10	0	None Visible
	1664	0.80	5.99	0	None Visible

TPS Type	Test #	AI Particle Diameter, cm	Velocity, km/sec	Impact Angle, degrees	Composite Tank Wall Damage
AFRSI	1603	0.32	6.20	0	1.1 x 0.6 cm Hole
	1605	0.32	6.80	0	None Visible
	1606	0.64	5.88	0	2.2 x 5.6 cm Hole
	1607	0.47	5.91	0	2.5 x 1.3 cm Hole
	1608	0.32	6.20	0	1.0 x 0.6 cm Hole
	1678	0.32	6.11	0	Pinhole
	1604	0.32	6.30	0	Rear-side Delam.
	1609	0.47	6.06	0	2.3 x 2.3 cm Hole
	1610	0.47	5.97	30	2.8 x 2.0 cm Hole
	1635	0.47	6.20	0	1.8 x 3.6 cm Hole
	1637	0.47	6.20	0	1.7 x 2.9 cm Hole
	1654	0.47	5.93	0	1.9 x 3.2 cm Hole
	1655	0.47	5.91	0	1.5 x 1.7 cm Hole
	1657	0.47	approx. 6	0	1.5 x 2.8 cm Hole
	1658	0.47	6.16	0	1.4 x 2.0 cm Hole
	1665	0.64	6.16	0	6.8 x 3.5 cm Hole
	1667	0.47	5.92	0	None Visible
	1672	0.47	5.85	0	3.3 x 2.0 cm Hole
	1673	0.47	5.76	0	1.0 x 1.8 cm Hole
	1631	0.47	6.20	0	None Visible
	1632	0.64	5.83	0	4 Holes
	1661	0.47	approx. 6	0	None Visible
	1663	0.64	approx. 6	0	0.2 cm Hole
	1674	0.47	5.83	0	2.1 x 2.1 cm Hole
	1677	0.32	6.06	0	None Visible
	1642	0.32	6.45	0	None Visible
	1643	0.32	6.31	0	None Visible
	1671	0.47	5.97	0	2.5 x 2.2 cm Hole

## PREDICTING DAMAGE AT HIGHER VELOCITIES

With results from analyses and even from tests at less than 8 km/s, approximations can be made of damage that will occur at projectile impact velocities in orbit, 14 - 20 km/s. When similar predictions result from different methods, the predictions remain unsubstantiated by tests at actual expected impact velocities, and should be regarded as preliminary. For the heat shield materials included in this study, the expected increase in hole diameter may be approximated several ways, although with low confidence.

For laminate composite PEEK and graphite/epoxy plates, Reference [14] proposed a model to predict the entry hole diameter as a function of projectile energy, target thickness and projectile diameter. To predict the hole growth with increasing velocity, the new hole diameter would be proportional to a function of the cubed root of the projectile energy. This relationship held true in an additional study by Taylor, Herbert and Kay [15]. Other references indicate hole diameter growth is proportional to a function of velocity, from hydrocode analyses of metal targets [16], from space station shielding tests (back wall hole growth) [17], and from tests below 8 km/s for thin metal plates [18]. None of these functions are directly applicable to the heat shield blankets and tiles in this study. However, as a first approximation, the proportionality of hole diameter to the cubed root of projectile energy, proposed for laminate composite materials, should provide a reasonable estimate. As an example, from Table 6, test # 1617 in AETB resulted in a hole diameter of 1.8 cm. If proportional to velocity, the hole at 16 km/s would be 5.1 cm diameter. If proportional to the cubed root of the projectile energy, the hole at 16 km/s would be 3.6 cm. Further analyses and tests at higher impact velocities are required for the heat shield materials in this study to improve confidence in approximating the resulting hole diameters.

## SUMMARY AND CONCLUSIONS

The three TPS hole diameter equations developed during this study correlate well with the test data for normal impacts at approximately 6 km/s impacts. The less subjective measurements and more consistent material properties through the thickness of the AETB tiles led to a higher correlation than for the FRSI and AFRSI blankets. The equations may be used in the evaluation of impacts suffered on-orbit, however with less confidence since on-orbit impacts will occur at varying impact angles, and particle shapes, materials, and sizes, and at higher impact velocities.

More research is required to fully understand the implications of the orbital debris environment on reentry vehicles. The limited scope of this study should be expanded to include variations of particle density, impact angle and impact velocity, as a minimum, to gain more insight into the survivability of reusable launch vehicles, orbiter-type vehicles, and crew return vehicles.

*Acknowledgments*—Thanks to Angela Nolen, Mary Hovater and Melanie McCain for their performance of the hypervelocity impact tests at MSFC's Space Debris Impact Facility, and for their untiring assistance in compiling the details of the test parameters and each test sample used in this study.

## REFERENCES

1. J.H. Robinson, et al, Meteoroid/orbital debris implications to a reusable launch vehicle thermal protection system. *AIAA Space Programs and Technologies Conference*, AIAA 95-3606 (1995).
2. Dave Wittman, Early on-orbit TPS debris impact tests. Rockwell Aerospace- Space Systems Division, Laboratory Test Report No. LTR 6552-4031 (1994).
3. J.K. Pulley, Test report - debris impact test report - delta testing. Rockwell Aerospace Space Systems Division Report No. Addendum SSD94D0330 (1995).
4. E.L. Christiansen, Advanced meteoroid and debris shielding concepts. *AIAA/NASA/DOD Orbital Debris Conference*, AIAA 90-1336 (1990).
5. B.G. Cour-Palais and J.L. Crews, Multishock concept for spacecraft shielding. *Int. J. Impact Engng*, **10**(1-4), 135-146 (1990).
6. J. Zwiener, A. Mount, K. Herren, A. Nettles, C. Semmel, and J. Sims, Enhanced Whipple bumper system: impact resistance of composite materials. *AIAA Space Programs and Technologies Conference*, AIAA 92-1589 (1992).
7. G.D. Olsen and A.M. Nolen, Advanced shield design for space station freedom. *Int. J. Impact Engng*, **14**(1-4), 541-549 (1993).
8. E.L. Christiansen, J.E. Williamsen, J.L. Crews, J.H. Robinson, and A.M. Nolen, Enhanced meteoroid and orbital debris shielding. *Int. J. Impact Engng* (1995).
9. R.A. Taylor, Space debris simulation facility for spacecraft materials evaluation. *SAMPE Quarterly*, **18**(2) (1987).
10. Larry Jay Friesen and Eric L. Christiansen, Hypervelocity impact tests of X-38 crew return vehicles (CRV) thermal protection materials, part II. JSC 27664, December (1996).
11. Larry Jay Friesen and James Whitney, Hypervelocity impact tests of shuttle material targets. JSC 27315, June (1996).
12. C. Loupias et al., Hypervelocity impacts of orbital debris on an advanced heat shielding material: comparison of ouranos computations to experimental results. *Int. J. Impact Engng*, **20** (1997).
13. Ching H. Yew and Rodney B. Kendrick, Study of damage in composite panels produced by hypervelocity impact. *Int. J. Impact Engng*, **5** (1987).
14. R.C. Tennyson and G.D. Shortliffe, Hypervelocity impact tests on composite boom structures for space robot application. *9th Canadian Aeronautics and Space Conference on Astronautics, Ottawa, Canada* (1996).
15. Emma A. Taylor, Mark K. Herbert and Laurie Kay, Hypervelocity impact on carbon fibre reinforced plastic (CFRP)/ aluminum honeycomb at normal and oblique angles. *Second European Conference on Space Debris, ESOC, Darmstadt, Germany* (1997).
16. Alan J. Watts and Dale Atkinson, Dimensional scaling for impact cratering and perforation. *Int. J. Impact Engng*, **17** (1995).
17. J. Williamsen and W. Schonberg, Empirical models for spacecraft damage from orbital debris penetration and effects on spacecraft survivability. *Second European Conference on Space Debris, ESOC Darmstadt, Germany* (1997).
18. V. C. Frost, Meteoroid damage assessment. NASA SP-8042 (1970).